Applied Physics Letters

Observation of the magnetoelectric reversal process of the antiferromagnetic domain

Cite as: Appl. Phys. Lett. **113**, 242404 (2018); https://doi.org/10.1063/1.5053925
Submitted: 27 August 2018 • Accepted: 24 November 2018 • Published Online: 13 December 2018

Yu Shiratsuchi, Shunsuke Watanabe, Hiroaki Yoshida, et al.

Observation of the magnetoelectric reversal process of the antiferromagnetic domain

Yu Shiratsuchi,[1,a)] Shunsuke Watanabe,[1] Hiroaki Yoshida,[1] Noriaki Kishida,[1] Ryoichi Nakatani,[1] Yoshinori Kotani,[2] Kentaro Toyoki,[2] and Tetsuya Nakamura[2]
[1]*Department of Materials Science and Engineering, Graduate School of Engineering, Osaka University, 2-1 Yamadaoka, Suita, Osaka 565-0871, Japan*
[2]*Japan Synchrotron Radiation Research Institute (JASRI/SPring-8), 1-1-1, Kouto, Sayo, Hyogo 679-5198 Japan*

(Received 27 August 2018; accepted 24 November 2018; published online 13 December 2018)

We investigated the switching process of the perpendicular exchange bias, which is driven by the magnetoelectric effect, by conducting magnetic domain observations using scanning soft X-ray magnetic circular dichroism microscopy. Isothermal and simultaneous application of magnetic and electric fields switches the perpendicular exchange bias polarity. The switching process proceeds by the nucleation and growth of reversed domains. The correspondence among the ferromagnetic/antiferromagnetic domains and exchange bias polarity indicates that interfacial antiferromagnetic spin/domain reversal is responsible for the magnetoelectric switching of the perpendicular exchange bias polarity. *Published by AIP Publishing*. https://doi.org/10.1063/1.5053925

Electric-field-induced magnetization switching is a low-power magnetization switching method used in spintronics devices. Among the techniques used to affect this type of magnetization switching, e.g., voltage control of magnetic anisotropy[1] and switching driven by ferroelectricity,[2] magnetization switching based on the inherent magnetoelectric (ME) effect can suppress the leakage current to $<10^{-2}$ A/cm^2 (Refs. 3–5) because of the high electric resistance of the ME substance. Switching time can be decreased to <10 ns.[5] The ME substance is usually an antiferromagnetic (AFM) material such as $TbMnO_2$[5] or $BaFeO_3$,[2,6,7] so interfacial exchange coupling with a spin-polarizable material [ferromagnetic (FM) metals[2–5,8–10] or heavy metals with strong spin-orbit interaction such as Pt[10–12]] is used to detect the interfacial AFM spins. Exchange coupling with the FM layer induces exchange bias,[13–15] and owing to its unidirectional nature, ME switching through the exchange bias ensures correspondence between the magnetization direction and electric field polarity. In other words, the exchange-biased FM layer traces the interfacial spin state and/or the magnetic domain state of the underlying ME-AFM layer.[2,16]

Cr_2O_3 is a fundamental and prototypical ME material[17,18] that induces a high perpendicular exchange bias exceeding 0.4 erg/cm^2.[19,20] Its coercivity can be suppressed to <50 Oe by selecting a suitable spacer layer for insertion at the FM/AFM interface.[21] Although ME switching of FM (or Pt)/Cr_2O_3 stacked films has been reported,[3–5,11,12] the mechanism of the switching process remains unclear. In this regard, a ME-driven magnetization reversal process has been reported for the in-plane exchange-biased system, CoFe/$BiFeO_3$.[2] In the FM/ME-AFM stacked system, the ME-controlled AFM domain state is detected via the FM domain state. Then, both magnetic domains must be spatially coupled, which is nontrivial. Element-specific investigation can be carried out using X-ray magnetic linear dichroism (XMLD).[22,23] However, the XMLD intensity is proportional to $\cos^2\theta$, where θ denotes the angle between the X-ray incidence and the spin orientation; the collinear spin structure cannot be distinguished by this technique. However, as the high perpendicular exchange bias is induced by the collinear spin structure, direct observation of the AFM domains is complicated. X-ray magnetic circular dichroism (XMCD) is proportional to $\cos\theta$, which mitigates this limitation. Herein, we report on ME switching in Pt/Co/Au/Cr_2O_3/Pt perpendicular exchange-biased films, by observing the magnetic domains using scanning XMCD microscopy with soft X-rays sensitive to the 3d elements.[16,24]

Pt/Co/Au/Cr_2O_3/Pt films (1.5/0.4/1.0/150/20 nm) were fabricated using DC magnetron sputtering. A twinned Pt(111) buffer layer was deposited at 873 K on an α-Al_2O_3(0001) substrate. Then, a twinned Cr_2O_3(0001) layer was fabricated by reactive sputtering at 773 K using an Ar and O_2 gas mixture. The Au, Co, and Pt layers were deposited sequentially at room temperature. The details of the structural information can be found in our previous paper.[21]

ME switching of the perpendicular exchange bias was characterized by anomalous Hall effect (AHE) measurements using a micro-fabricated Hall device (width: 10 μm and length: 50 μm). An optical micrograph of the device with the setup for AHE measurements is shown in Fig. 1. ME switching requires simultaneous application of the magnetic and electric fields.[3–5,8–12] These fields were applied perpendicular to the film plane, with the down-up direction (i.e., from the bottom to top electrode) defined as positive. The electric field E (voltage V) was varied from −1226 kV/cm (−19 V) to +1333 kV/cm (+20 V), whereas the magnetic field H was maintained constant at +40 kOe. For all measurements and observations, the sample was initialized to the saturated state, i.e., the fully positive or negative exchange-biased state, before the application of E and H. After removing E and H, the exchange bias field H_{EB} and remanence

[a)]Author to whom correspondence should be addressed: shiratsuchi@mat.eng.osaka-u.ac.jp

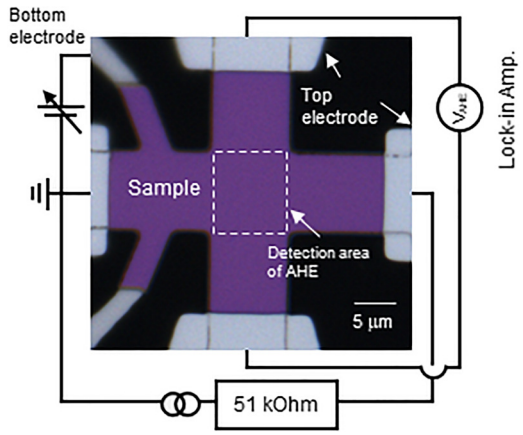

FIG. 1. Optical microscopy image of the micro-Hall device, including a schematic drawing of the electrical circuit for the AHE measurements. The top electrodes were used for the detection of the TEY signal for XMCD imaging. The purple, white, and black regions correspond to the sample, electrode, and substrate.

ratio M_R/M_S were checked by measuring the AHE loops as a function of the magnetic field in the range of ± 1.5 kOe under no electric field. AHE measurements were carried out at 280 K after cooling the sample from 310 K under a magnetic field of +6 kOe.

Using the Hall device on the same samples used for AHE measurements (see Fig. 1), magnetic domain observation was carried out using scanning XMCD microscopy (BL25SU, SPring-8 Japan). The soft X-ray beam was focused with a size of approximately 100 nm on the film surface using a Fresnel zone plate. The incident soft X-ray photon energy was 778.6 eV at the Co L_3 edge or 576.1 eV at the Cr L_3 edge, and the incidence direction was normal to the surface. The perpendicular component of the FM and AFM spins was detected. The XMCD signal was collected as the difference in the absorption of soft X-rays with positive (μ_+) and negative (μ_-) helicities, where $\mu_+ - \mu_-$ was measured by the total electron yield (TEY) method. To obtain the two-dimensional distribution of the XMCD intensity, the two-dimensional distribution of the absorption intensity, $\mu_+ + \mu_-$, was compensated for, thereby enabling the normalized XMCD intensity, $(\mu_+ - \mu_-)/(\mu_+ + \mu_-)$, to be mapped. The substrate regions were trimmed from each obtained image, because no TEY signal was detectable there. Details of the scanning XMCD microscope and the detection method can be found in Refs. 16 and 24. Observations were carried out in the remanence state, i.e., $H = 0$ Oe and $E = 0$ V/cm. The measurement temperature and the cooling protocol were the same as in the AHE measurements.

We first present the results of ME switching, based on the AHE measurements. Figure 2(a) shows the typical AHE loops before and after switching. In the initial state, i.e., immediately after field cooling, the AHE loop is almost the same as the loop with a negative exchange bias (blue curve) because the field was cooled under positive H. After applying fields of $H = +40$ kOe and $E = +1333$ kV/cm, a positive exchange bias is observed, i.e., negative-to-positive switching. Starting from the positive exchange-biased state, the application of $H = +40$ kOe and $E = -800$ kV/cm switched the exchange bias polarity from positive to negative again,

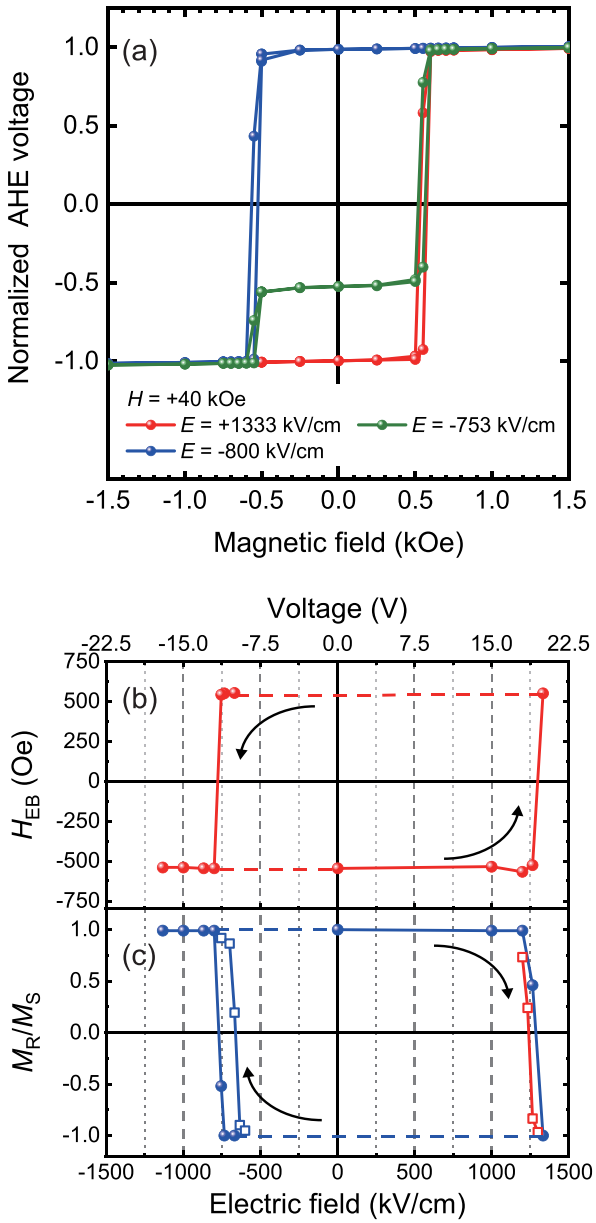

FIG. 2. (a) AHE loops before and after ME switching. The red, blue, and green curves represent measurements after applying $H = +40$ kOe, $E = +1333$ kV/cm (positive exchange bias) and $H = +40$ kOe, $E = -800$ kV/cm (negative exchange bias), and $H = +40$ kOe, $E = -753$ kV/cm (intermediate), respectively. In (b) and (c), hysteresis of the perpendicular exchange bias field H_{EB} and the remanence ratio M_R/M_S as a function of the applied electric field were shown, respectively. H_{EB} and M_R/M_S (plotted on the left and right axes, respectively), were measured at 280 K. Before applying H and E, the film was initialized to the saturated state (see the text). The arrows in (b) and (c) represent the direction of the process. The open symbols in (c) represent the M_R/M_S estimated from the domain images (shown in Fig. 3). The blue and red squares represent the values estimated from Figs. 3(a) and 3(b), respectively.

i.e., positive-to-negative switching. As previously reported,[5,9] this isothermal switching is fully reversible, demonstrated by the clear hysteresis in H_{EB} and M_R/M_S as a function of E [Fig. 2(b)]. In the intermediate state, a two-step AHE loop is observed [green curve in Fig. 2(a)], which can be interpreted as coexistence of positive and negative exchange-biased regions. The ratio of states is reflected in the value of M_R/M_S. Then, the threshold electric fields E_{TH} are defined as E values at which $M_R/M_S = 0$ and $E_{TH} = -770^{+20}_{-30}$ kV/cm for positive-to-negative switching and $+1280^{+50}_{-20}$ kV/cm for negative-to-

positive switching. The difference in E_{TH} values is attributed to the unidirectional nature of the exchange magnetic anisotropy, namely the exchange bias effect acting on the interfacial AFM spins. The H-dependence of the energy condition at the threshold is discussed in our previous reports.[25] In this report, we focus on the E-dependence of the magnetization reversal process.

The intermediate magnetic domain state, i.e., the coexistence state, is shown in Fig. 3. To ensure the change in XMCD contrast is clear, a histogram of XMCD intensity is shown for each image; the peak at approximately XMCD ≈ 0 corresponds to the contrast from the electrode. A multi-domain state is clearly observed. For both the positive-to-negative and the negative-to-positive switching processes, an increase in the absolute values of E leads to an expansion of the reversed region, indicating that ME switching involves nucleation and growth of the reversed magnetic domain. In the negative-to-positive switching process, the reversed domain nucleates at the edge of the Hall device. In contrast, in the positive-to-negative switching process, nucleation occurs at both the edge (indicated by A) and the center (indicated by B) of the Hall device. Consequently, the reversal process is asymmetric for positive-to-negative and negative-to-positive switching. Asymmetric magnetization reversal under magnetic-field cycling was observed in the exchange-biased FM layer.[26] The nucleation of the reversed domain at the edge of the device implies that the AFM domain reversal is affected by the demagnetization field. This is reasonable considering that the driving force for AFM domain reversal is the Zeeman energy of the magnetization induced by the E-field. It is possible that the magnetic anisotropy energy is reduced at the edge because of damage inflicted during micro-fabrication; however, the exchange bias field would then also be reduced at the edge, leading to nucleation of the reversed domain by the magnetic field sweep, i.e., ordinal magnetic hysteresis at zero E. In contrast, we confirmed that the reversed domains nucleate randomly on the device, indicating that the above-mentioned effect is not significant.

We should mention the difference in the absolute values of E in the reversal process. In Fig. 2(c), the ratio of blue/red domains, corresponding to M_R/M_S as a function of E is shown as the open symbols. The ratio roughly matches M_R/M_S estimated from the AHE measurements, whereas the absolute values of E differ slightly for two loops. This is partly because only the magnetic state in the crossed area (the dotted area in Fig. 1) is detected by AHE measurements,

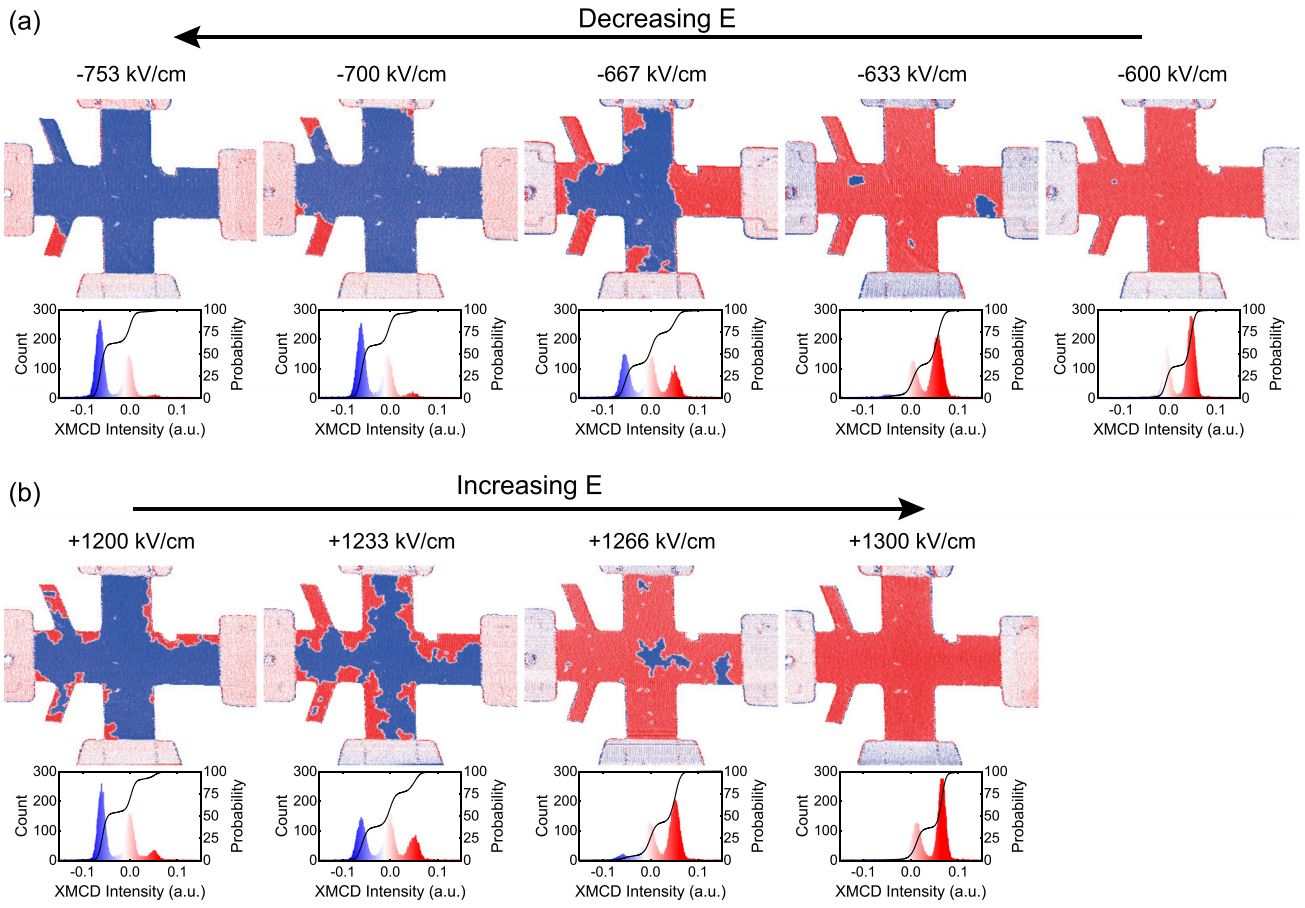

FIG. 3. Spatial distributions of XMCD intensity at the Co L_3 edge, corresponding to the ferromagnetic domain after applying H (=+40 kOe) and E. (a) and (b) represent the change in the spatial distribution of the XMCD intensity in decreasing and increasing branches of Fig. 2(b). Histograms of the XMCD intensity are also shown. The line in the histogram represents the integrated frequency curve. Before applying H and E, the film was initialized to the saturated state (see the text). The measurement temperature was 280 K. The positions indicated by A and B are the nucleation sites of the reversed domain at $E = -600$ kV/cm (-9 V). The substrate regions were trimmed from each image.

whereas the magnetic domain observation covers the whole Hall device. It is also noteworthy that the reversed region indicated by A vanishes at −667 kV/cm (−10.0 V). This is probably because of the latency associated with thermally activated reversed domain nucleation. In this work, the sample was initialized before applying H and E for each image; consequently, nucleation of the reversed domain would occur stochastically.

The images shown in Fig. 3 were observed at the Co L_3 edge. They correspond to the FM domain. However, the observed change in the magnetic domain pattern is driven by interfacial uncompensated AFM spin and/or AFM domain reversal. The ME switching event occurs under simultaneous application of magnetic and electric fields. In fact, the magnetization switching does not occur by the application of the magnetic field of +40 kOe alone; this is also understood from the clear hysteresis of Fig. 2(b). Furthermore, since the magnetic field during the switching event (+40 kOe) is sufficiently higher than the saturation field of the FM layer [see Fig. 2(a)], the FM magnetization is fixed during the switching event. In this work, the magnetic field was not applied in the negative direction before the magnetic domain observation, and the M_R/M_S of Co is unity. Thus, the positive exchange bias is the sole driving force of the magnetization reversal of FM Co when H decreases from +40 kOe to 0 Oe.

Further verification is possible by showing the exchange bias polarity is (1) determined in a domain-by-domain manner and (2) coupled with interfacial uncompensated AFM spin and/or AFM domain. In Figs. 4(a) and 4(b), we show the magnetic domain pattern of FM Co and the local element-specific magnetization curves (L-ESMCs) measured by scanning XMCD microscopy after zero-field cooling. The sample used here had slightly different thickness Au-spacer and Pt-capping layers (0.5 and 1.2 nm, respectively), to control the perpendicular magnetic anisotropy energy density and resultant magnetic domain size. It should be noted that the beam position fluctuated by a few micrometers during L-ESMC measurements. The L-ESMCs for the red and blue Co domains (indicated by positions X and Y, respectively) exhibit a negative and positive exchange bias, respectively. In our sample, because H_{EB} exceeds the coercivity, the remanent magnetic domain pattern corresponds to the spatial distribution of the exchange bias polarity. The spatial distributions of the XMCD intensity measured at the Co L_3 and Cr L_3 edges are shown in Figs. 4(c) and 4(d), respectively. The former corresponds to the FM domain described above. The XMCD signs of Co and Cr are opposite because of interfacial AFM coupling.[27] The similarity of the two patterns indicates that the FM domain pattern is a tracing of the spatial distribution of the interfacial uncompensated AFM spins. Additionally, we confirmed that the remanence state magnetic domain pattern is robust against magnetic field cycling. The magnetization process for magnetic field cycling is beyond the scope of this paper, and will be reported elsewhere. Combined with the results shown in Figs. 4(a) and 4(b), the exchange bias polarity couples with the direction of the interfacial uncompensated AFM spins. Considering that the collinear spin is aligned along the c-axis of Cr_2O_3,[28] the image shown in Fig. 4(d) may correspond to the AFM domain pattern. Then, the above discussion strongly supports that the magnetization reversal processes shown in Fig. 3 are driven by the reversal of interfacial uncompensated AFM spins and/or AFM domains. The results presented in this paper indicate that the ME-driven AFM spin/domain reversal is similar to that of an ordinal ferromagnet. This is consistent with the recent report by Iyama and Kimura in which ME Cr_2O_3 exhibits a ferroic feature under a constant E or H.[29]

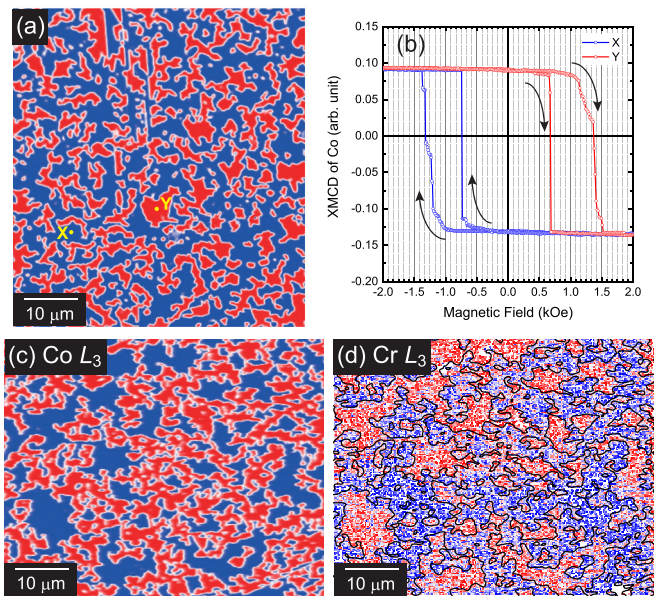

FIG. 4. (a) Spatial distributions of XMCD at the Co L_3 edge after zero-field cooling and (b) the element-specific magnetization curve measured at positions X and Y. The arrows in (b) represent the direction of the magnetic-field cycling. (c) and (d) are the spatial distributions of XMCD intensity measured at the Co L_3 edge and Cr L_3 edge, respectively, observed at a position different from that in (a). The sample used for these measurements was the Pt(1.2)/Co(0.4)/Au(0.5)/Cr_2O_3(150)/Pt(20) film. The magnetic domain boundary in (c) is shown in (d) by using a thin black line as a guide to the eye. The measurement temperature was 280 K.

Our results demonstrate that ME switching of perpendicular exchange-biased systems happens by domain wall propagation in Cr_2O_3. By altering the electric field (voltage) from the DC field adopted herein to a pulse field, we could perhaps address the domain wall dynamics. According to the collective coordinate formalism,[30–32] the maximum mobility can reach 0.2–0.7 m/(s·Oe). In our system, the damping constant may be enhanced because of interfacial exchange coupling with the FM layer, which may limit the domain wall velocity.[5] Further investigation of the domain wall dynamics will be reported elsewhere.[33] Another remaining problem is the operating temperature. To solve this, improvement of the Neél temperature of the Cr_2O_3 layer[34] would be required; this is out of scope of this paper.

In summary, we investigated the reversal process of the perpendicular exchange bias polarity driven by the ME effect of Cr_2O_3 in a Pt/Co/Au/Cr_2O_3/Pt Hall device. ME switching was shown to proceed by the nucleation and growth of reversed interfacial uncompensated AFM spins and/or reversed AFM domains. The reversal process was asymmetric with respect to the direction of the applied electric field; (1) the nucleation sites of the reversed domain and (2) the

absolute value of the switching E-field differed in the decreasing (positive-to-negative) and increasing (negative-to-positive) E-fields. These results indicate that electric-field induced magnetization reversal in ME Cr_2O_3 is similar to exchange-biased FM magnetization.

The magnetic domain observations using the scanning XMCD microscope were carried out with the approval of the JASRI (Proposal Nos. 2016A0079, 2016B0079, and 2017A0079). This work was partly supported by JSPS KAKENHI Grant Nos. 16H03832, 16H02389, and 18K18311, ESICMM (Elements Strategy Initiative Center for Magnetic Materials) is funded by the Ministry of Education, Culture, Sports, Science and Technology, the Elements Strategy Initiative Center for Magnetic Materials (MEXT), and the Photonics Advanced Research Center (PARC) at Osaka University.

[1]T. Maruyama, Y. Shiota, T. Nozaki, K. Ohta, N. Toda, M. Mizuguchi, A. A. Tulapurkar, T. Shinjo, M. Shiraishi, S. Mizukami, Y. Ando, and Y. Suzuki, Nat. Nanotechnol. **4**, 158 (2009).
[2]Y.-H. Chu, L. W. Martin, M. B. Holcomb, M. Hajek, S.-J. Han, Q. He, N. Balke, C.-H. Yang, D. Lee, W. Hu, Q. Zhan, P.-L. Yang, A. Fraile-Rodrígues, A. Scholl, S. X. Wang, and R. Ramesh, Nat. Mater. **7**, 478 (2008).
[3]T. Ashida, M. Oida, N. Shimomura, T. Nozaki, T. Shibata, and M. Sahashi, Appl. Phys. Lett. **106**, 132407 (2015).
[4]K. Toyoki, Y. Shiratsuchi, A. Kobane, C. Mitsumata, Y. Kotani, T. Nakamura, and R. Nakatani, Appl. Phys. Lett. **106**, 162404 (2015).
[5]T. V. A. Nguyen, Y. Shiratsuchi, and R. Nakatani, Appl. Phys. Express **10**, 083002 (2017).
[6]T. Arima, J. Phys. Soc. Jpn. **80**, 052001 (2011).
[7]D. Heron, D. G. Schlom, and R. Ramesh, Appl. Phys. Rev. **1**, 021303 (2014).
[8]P. Borisov, A. Hochstrat, X. Chen, W. Kleemann, and C. Binek, Phys. Rev. Lett. **94**, 117203 (2005).
[9]X. Chen, A. Hochstrat, P. Borisov, and W. Kleemann, Appl. Phys. Lett. **89**, 202508 (2006).
[10]X. He, N. Wu, A. N. Caruso, E. Vescovo, K. D. Belashchenko, P. A. Dowben, and C. Binek, Nat. Mater. **9**, 579 (2010).
[11]T. Kosub, M. Kopte, F. Radu, O. G. Schmitdt, and D. Makarov, Phys. Rev. Lett. **115**, 097201 (2015).
[12]T. Kosub, M. Kopte, R. Hühne, P. Appel, B. Shields, P. Maltinsky, R. Hübner, M. O. Liedke, J. Fassbender, O. G. Schmidt, and D. Makarov, Nat. Commun. **8**, 13985 (2017).
[13]W. H. Meiklejohn and C. P. Bean, Phys. Rev. **102**, 1413 (1956); **105**, 904 (1957).
[14]J. Nogués and I. K. Schuller, J. Magn. Magn. Mater. **192**, 203 (1999).
[15]A. E. Berkowitz and K. Takano, J. Magn. Magn. Mater. **200**, 552 (1999).
[16]Y. Shiratsuchi, Y. Kotani, S. Yoshida, Y. Yoshikawa, K. Toyoki, A. Kobane, R. Nakatani, and T. Nakamura, AIMS Mater. Sci. **2**, 484 (2015).
[17]D. N. Astrov, JETP **10**, 628 (1960).
[18]V. J. Folen, G. T. Rado, and E. W. Stadler, Phys. Rev. Lett. **6**, 607 (1961).
[19]Y. Shiratsuchi, T. Fujita, H. Oikawa, H. Noutomi, and R. Nakatani, Appl. Phys. Express **3**, 113001 (2010).
[20]Y. Shiratsuchi and R. Nakateni, Mater. Trans. **57**, 781 (2016).
[21]Y. Shiratsuchi, W. Kuroda, T. V. A. Nguyen, Y. Kotani, K. Toyoki, T. Nakamura, M. Suzuki, K. Nakamura, and R. Nakatani, J. Appl. Phys. **121**, 073902 (2017).
[22]F. Nolting, A. Scholl, J. Stöhr, J. W. Seo, J. Fompeyrfine, H. Siegwart, J.-P. Locquet, S. Anders, J. Lüning, E. E. Fullerton, M. F. Toney, M. R. Scheinfein, and H. A. Padmore, Nature **405**, 767 (2000).
[23]L. Duò, M. Finazzi, and F. Ciccacci, *Magnetic Properties of Antiferromagnetic Oxide Materials* (Wiley-VCH, Weinheim, 2010), Chap. 8.
[24]Y. Kotani, Y. Senba, K. Toyoki, D. Billington, H. Okazaki, A. Yasui, W. Ueno, H. Ohashi, S. Hirosawa, Y. Shiratsuchi, and T. Nakamura, J. Synchrotron Radiat. **25**, 1444 (2018).
[25]T. V. A. Nguyen, Y. Shiratsuchi, A. Kobane, S. Yoshida, and R. Nakatani, J. Appl. Phys. **122**, 073905 (2017).
[26]Q. Wu, W. He, H.-L. Liu, Y.-F. Liu, J.-W. Cai, and Z.-H. Cheng, J. Appl. Phys. **113**, 033901 (2013).
[27]Y. Shiratsuchi, H. Noutomi, H. Oikawa, T. Nakamura, M. Suzuki, T. Fujita, K. Arakawa, Y. Takechi, H. Mori, T. Kinoshita, M. Yamamoto, and R. Nakatani, Phys. Rev. Lett. **109**, 077202 (2012).
[28]L. M. Corliss, J. M. Hastings, R. Nathans, and G. Shirane, J. Appl. Phys. **36**, 1099 (1965).
[29]A. Iyama and T. Kimura, Phys. Rev. B **87**, 180408(R) (2013).
[30]E. G. Tveten, A. Qaiumzadeh, O. A. Tretiakov, and A. Brataas, Phys. Rev. Lett. **110**, 127208 (2013).
[31]K. D. Belashchenko, O. Tchernyshyov, A. A. Kovalev, and O. A. Tretiakov, Appl. Phys. Lett. **108**, 132403 (2016).
[32]R. Zarzuela, S. K. Kim, and Y. Tserkovnyak, Phys. Rev. B **97**, 014418 (2018).
[33]Y. Shiratsuchi, H. Yoshida, Y. Kotani, K. Toyoki, T. V. A. Nguyen, T. Nakamura, and R. Nakatani, "Antiferromagnetic domain wall creep driven by magnetoelectric effect" APL Mater. (to be published).
[34]M. Street, W. Echtenkamp, T. Komesu, S. Cau, P. A. Dowben, and C. Binek, Appl. Phys. Lett. **104**, 222402 (2014).